Alsumiri *et al. Protection and Control of Modern Power Systems* (2018) 3:24
https://doi.org/10.1186/s41601-018-0097-x

Protection and Control of Modern Power Systems

ORIGINAL RESEARCH Open Access

Residue Theorem based soft sliding mode control for wind power generation systems

Mohammed Alsumiri, Liuying Li*, Lin Jiang and Wenhu Tang

Abstract

This paper proposes a residue theorem based soft sliding mode control strategy for a permanent magnet synchronous generator (PMSG) based wind power generation system (WPGS), to achieve the maximum energy conversion and improved in the system dynamic performance. The main idea is to set a soft dynamic boundary for the controlled variables around a reference point. Thus the controlled variables would lie on a point inside the boundary. The convergence of the operating point is ensured by following the Forward Euler method. The proposed control has been verified via simulation and experiments, compared with conventional sliding mode control (SMC) and proportional integral (PI) control.

Keywords: Maximum power point tracking, Sliding mode control, Residue theorem, Wind power generation system, Permanent magnet synchronous generator

1 Introduction

Wind energy is growing fast in the world and is one of the most explored renewable energy sources. The control strategy of WPGS can affect the amount of extracted power from the wind [1]. The wind is a source of energy which is highly affected by the uncertain fluctuations. As a result, wind power generation system can be described as a complex nonlinear system operates in highly uncertain environments which demand a tight control management [2]. The control system of WPGS plays an important role to affect the amount of extracted power from wind. WPGSs need the controller to make MPPT process has fewer overshoots in the speed response and smooth transit between different operation regions [3].

SMC has been investigated for WPGS due to its robustness and simple structure [4]. Elimination of chattering effect is an area of concern when implementing SMC. Although this can be avoided by a slight change in the sliding mode dynamics, it has been deduced in [5] that the discontinuity dynamics change the ultimate robustness and accuracy of the sliding mode nature are partially lost.

This paper proposes Residue Theorem based soft sliding mode control for wind power generation systems to improve the energy conversion ratio and the dynamic performance with a better ability to handle the uncertainties. There are two controllers developed with different boundary definition in this paper. The main idea is to set a soft dynamic boundary for controlled variables around a reference point, so that controlled variables lie on a point inside the boundary. The soft dynamic boundary will keep the control signal continuous. The soft changing manner of the boundary allows the speed to settle in reduced damping, and this prevents the WPGS from a mechanical shaft stress and damage. During transient state, as a PMSG accelerating the generated control boundary decreases smoothly, since the generated control boundary depends on the difference between the actual and reference speeds. Then at steady state, the generated control boundary become almost zero. Also, a wind speed estimation algorithm is designed and implemented which provides a solution with the wind speed measurement.

This paper is organised as the following: The first section presents the modelling of PMSG based WPGS. Then WPGS with PI control is illustrated. Besides, SMC is developed for a PMSG based WPGS. The residual control method and the design of the two controllers is shown and explained in this paper. In one controller the proposed method is implemented in the speed control loop of the PMSG, where in the second controller

*Correspondence: liuying@liv.ac.uk
University of Liverpool, Liverpool, UK

the proposed control method is implemented in speed and dq-axis currents control loops. Also in this section, a wind speed estimation algorithm is proposed and implemented in the WPGS controller. After that, the simulation results and analysis is presented. Also, the comparison between residual and SM controller is undertaken. Following the simulation results, the experimental verification are illustrated to validate the proposed control strategy. The whole paper is concluded in the final section.

2 System model and vector control with PI

The investigated WPGS, shown in Fig. 1a, consists of a vertical axial wind turbine (VAWT) coupled directly to a sinusoidal back-EMF PMSG. The output of the PMSG is connected to an uncontrolled AC/DC rectifier. The DC output of the rectifier is connected to a DC/DC boost converter. The boost converter is operating in the continuous conduction mode.

The output power of a wind turbine is the extracted kinetic energy stored in wind multiplied by a power coefficient. The wind power is directly proportional to the cube of wind speed [6].

$$P_w = \frac{1}{2}\rho A V_w^3, \tag{1}$$

The extracted mechanical power is calculated as multiplying the wind power by a power coefficient as follows:

$$P_m = \frac{1}{2}\rho C_p A V_w^3. \tag{2}$$

The calculation of a power coefficient C_p depends on wind turbine types, i.e. vertical axis and horizontal axis wind turbine. C_p is a function of the tip speed ratio λ and the pitch angle of the blade. This relationship is normally

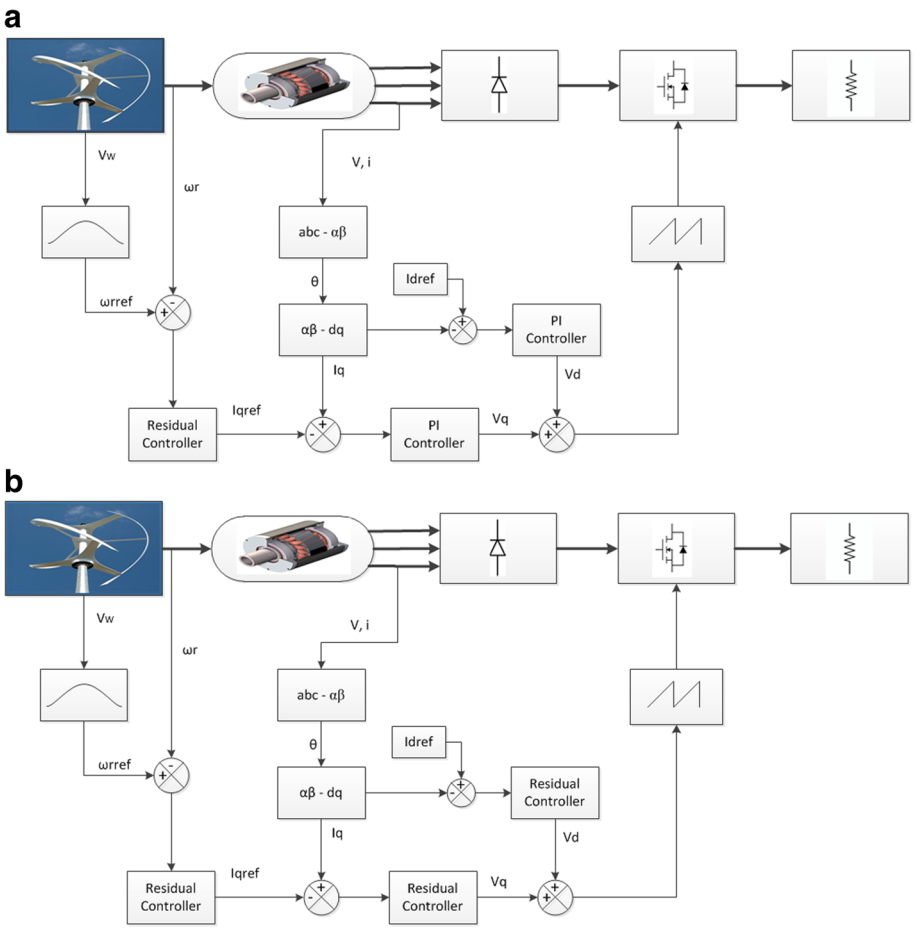

Fig. 1 System description and control. **a** Wind generator system description and control of Residual for speed controller. **b** The control diagram of Residual for speed and currents controller

provided by the wind turbine manufacturers. In order to approximate the value of the power coefficient, polynomials method were introduced [7]. Generally, for small-scale WPGSs the pitch angle is fixed to avoid the high cost of controlling mechanical pitch angles. In this research the equation which relates C_p and TSR is given as the following [6]:

$$C_p = -0.13\lambda^3 - 0.12\lambda^2 + 0.45\lambda, \qquad \lambda = \frac{\omega_r R}{V_w}, \tag{3}$$

By solving Eq. (3) for a TSR from 0 to 2, the WPGS can extract the maximum power from the wind when the TSR is equal to 0.82 and the maximum C_p is 0.221.

2.1 PMSG Model

The PMSG can be modelled in the dq-synchronous reference frame. The d-axis is aligned with the magnet axis, and the q-axis is orthogonal to the d-axis with respect to the direction of rotation [8]. The representation of the PMSG in the $d-q$ synchronous reference is shown as below:

$$\left.\begin{aligned} V_d &= R_s i_d + L_d \tfrac{di_d}{dt} - \omega_e L_q i_q, \\ V_q &= R_s i_q + L_q \tfrac{di_q}{dt} + \omega_e (L_d i_d + \psi_{PM}). \end{aligned}\right\} \tag{4}$$

The mechanical behavior of the PMSG can be described as the following:

$$\left.\begin{aligned} T_m &= T_e + J\tfrac{d\omega_r}{dt} + B\omega_r, \\ \omega_e &= p\omega_r, \\ T_e &= 1.5p(\psi_{PM} i_q + (L_d - L_q) i_d i_q), \end{aligned}\right\} \tag{5}$$

In order to implement vector control strategy, the linearization of the voltage equation is necessary. The linearization of the PMSG model is done by removing the cross-coupling between the dq-axis voltages [9]. This cross coupling can be seen in voltage equations in terms of $-\omega_e L_q i_q$ and $\omega_e(L_d i_d + \psi_{PM})$ for d-axis and q-axis respectively. The dq-axis voltages equations after removing the cross-coupling are as follow:

$$V_d = R_s i_d + L_d \frac{di_d}{dt}, \tag{6}$$

$$V_q = R_s i_q + L_q \frac{di_q}{dt}. \tag{7}$$

2.2 Vector control with PI

Proportional and Integral controllers are commonly used in control applications since they are easy to design, implement and tune. However, in WPGS classical PI controllers might not be the desired control strategy as it becomes difficult to handle uncertainties in nonlinear environments. So that the achievement of efficient and robust operations can not guaranteed. Generally, the idea of PI controller is to regulate the error between the measured input and the desired output. This error along with its integral provide a signal for the controller action with respect to time [10].

In this application, PI control strategy has been implemented to investigate the system dynamics and to compare them with advanced control strategies. In WPGS application, the PI controller has been employed to PMSG after removing the cross-coupling between the d-axis and q-axis circuits. The linear model after adding the decoupling voltages, which remove the cross-coupling to improve the system dynamic performance, to the system can be shown in (6) and (7). The structure of the PI controller can be shown as follows [10]:

$$G(s) = k_p + \frac{k_i}{s}, \tag{8}$$

The closed loop transfer functions of the speed control, the d-axis and q-axis currents control can be shown in Fig. 2, which illustrates the linearized model of a PMSG with PI speed and current controllers.

3 Maximum power point tracking controller using sliding mode control

Sliding mode control has the advantages of quick response and robustness. It can be defined as a variable structure control strategy based on the feedback and high frequency switching control [11]. Moreover, it is insensitive to system parameter changes, disturbances and load variations [12]. The design of SMC consists of two main stages. The first stage is to achieve the design of a stable sliding surface. The second stage aims to obtain an optimum design of a control law, which forces system operating points to reach a predetermined surface in finite time [13, 14].

3.1 Speed controller design

A speed controller is designed in order to achieve a reference optimal value of rotation speed ω_r, which is the optimal rotation speed. Consequently, a maximum power extraction can be obtained. The mechanical speed error is defined as the difference between the actual mechanical speed of PMSG and the reference speed ω_{rref} generated from an MPPT controller, which is expressed as follows:

$$e_1 = \omega_{rref} - \omega_r. \tag{9}$$

For $n = 1$, the sliding surface can be obtained then the speed controller can be designed as the following:

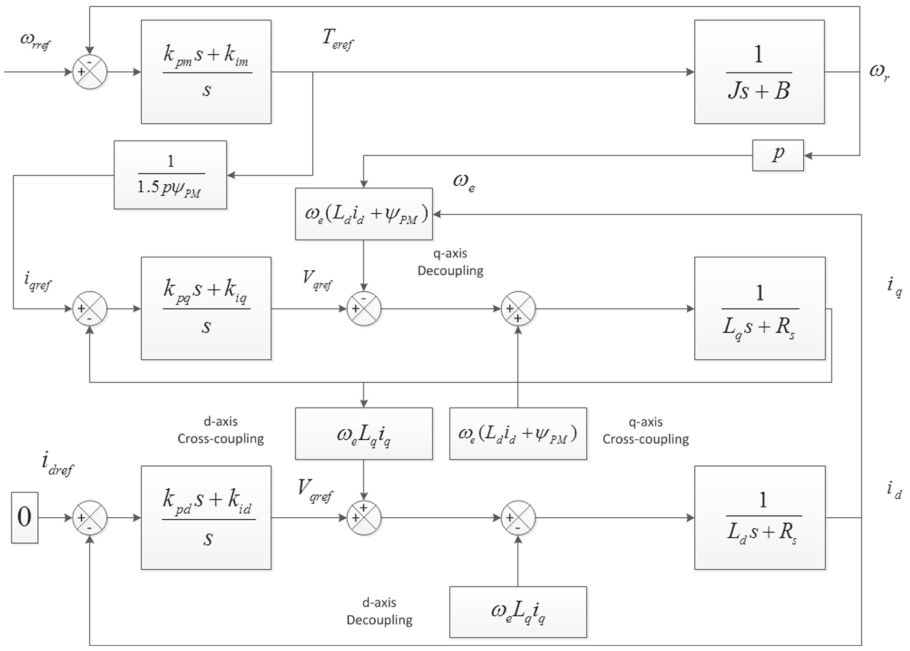

Fig. 2 Block diagram of the linearised model of a PMSG with PI speed and current controllers

$$\left.\begin{aligned} s(\omega_r) &= e,\\ \dot{s}(\omega_r) &= \dot{\omega}_{rref} - \tfrac{1}{J}T_m + \tfrac{1}{J}T_e + \tfrac{B}{J}\omega_r,\\ \dot{s}(\omega_r) &= \dot{\omega}_{rref} - \tfrac{1}{J}T_m + \tfrac{1.5p\psi_{PM}}{J}i_q + \tfrac{B}{J}\omega_r,\\ u_{eq} &= i_q^{eq} = \tfrac{J}{1.5p\lambda_{PM}}(\tfrac{1}{J}T_m - \dot{\omega}_{rref} - \tfrac{B}{J}\omega_r). \end{aligned}\right\} \quad (10)$$

The proposed speed controller is derived as (11).

$$u_1 = \frac{J}{1.5p\lambda_{PM}}\left(\frac{1}{J}T_m - \dot{\omega}_{rref} - \frac{B}{J}\omega_r) - K_\omega sgn(e_1\right). \quad (11)$$

3.2 Direct current controller design

To implement the Field Orientated Control (FOC) [15], the direct current or the d-axis current is set to zero. So the d-axis current error is the difference between the actual d-axis current and zero, which is expressed as below:

$$e_2 = i_{dref} - i_d, \qquad i_{dref} = 0. \quad (12)$$

For $n = 1$, the sliding surface can be obtained. Hence, the d-axis current controller can be designed as follows:

$$\left.\begin{aligned} s(i_d) &= e\\ \tfrac{di_d}{dt} &= \tfrac{1}{L_d}(V_d - R_a i_d + L_d\omega_e i_q),\\ \dot{s}(i_d) &= \dot{i}_{dref} - \tfrac{V_d}{L_d} + \tfrac{R_a}{L_d}i_d - \omega_e i_q,\\ u_{eq} &= V_d^{eq} = L_d(\dot{i}_{dref} + \tfrac{R_a}{L_d}i_d - \omega_e i_q). \end{aligned}\right\} \quad (13)$$

The proposed direct current controller design is shown in (14).

$$u_2 = L_d\left(\dot{i}_{drref} + \frac{R_a}{L_d}i_d - \omega_e i_q\right) - K_d sgn(e_2). \quad (14)$$

3.3 Quadrature current controller design

The quadrature current controller is used in order to obtain a q-axis reference voltage. The reference quadrature current, which is generated from the speed controller, is compared to the actual q-axis current of the PMSG to obtain the q-axis current error. It is expressed as below:

$$e_3 = i_{qref} - i_q. \quad (15)$$

For $n = 1$, the sliding surface can be obtained and the controller can be designed as the following:

$$\left.\begin{aligned} s(i_q) &= e\\ \tfrac{di_q}{dt} &= \tfrac{1}{L_q}(V_q - R_a i_q - L_q\omega_e i_d - \omega_e\psi_{PM}),\\ \dot{s}(i_q) &= \dot{i}_{qref} - \tfrac{V_q}{L_q} + \tfrac{R_a}{L_q}i_q + \omega_e i_d + \omega_e\tfrac{\psi_{PM}}{L_q},\\ u_{eq} &= V_q^{eq} = L_q(\dot{i}_{qref} + \tfrac{R_a}{L_q}i_q + \omega_e i_d + \omega_e\tfrac{\psi_{PM}}{L_q}), \end{aligned}\right\} \quad (16)$$

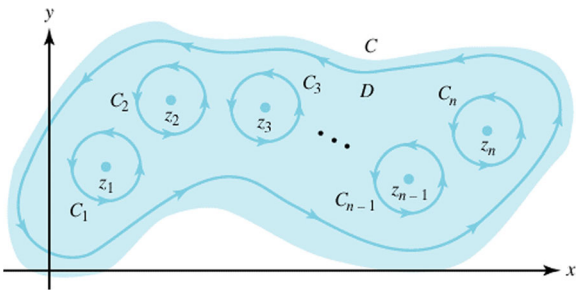

Fig. 3 Illustration of the Cauchy's Residue Theorem

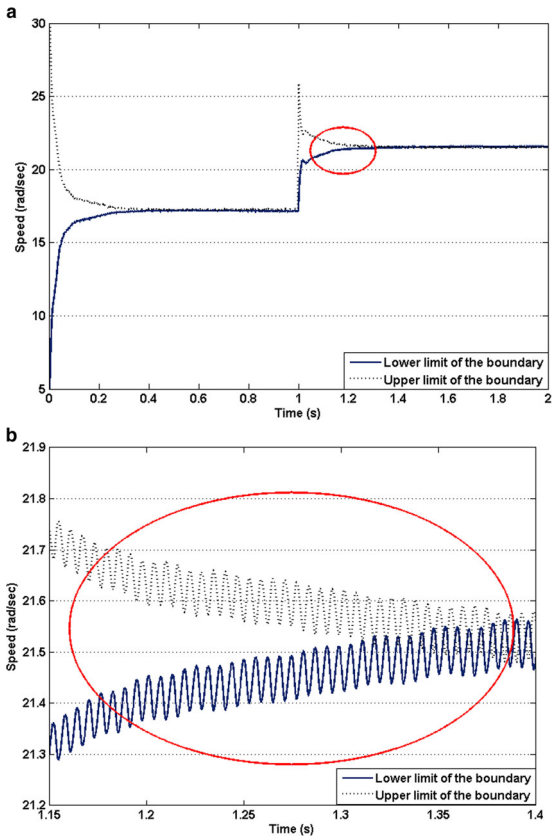

Fig. 4 The proposed dynamic speed Control boundary based on Cauchy's Residue Theorem **a** The designed speed control boundary based on Residue Theorem. **b** Zoom in the designed speed control boundary

The proposed quadrature direct current controller design is derives as (17).

$$u_3 = L_q\left(\dot{i}_{qref} + \frac{R_s}{L_q}i_q + \omega_e i_d + \omega_e\frac{\psi_{PM}}{L_q}\right) - K_q sgn(e_3). \tag{17}$$

Finally, the values of the d-axis and q-axis voltages are used in order to generate a control signal using pulse width modulation (PWM).

4 Residue theorem based SMC

4.1 Residue theorem

The residue theorem is considered as one of the best tools to predict the area under a curve. The Cauchy Theorem stated that if a function is analytic on and in a closed contour C, then the integral over the closed contour is zero [16, 17].

Theorem 1. *Let D be a simply connected domain, and let C be a simple closed positively oriented contour that lies in D. If $f(z)$ is analytic inside and on C, except at the points $z_1, z_2, ..., z_n$ that lie inside C, then*

$$\oint f(z)dz = 2\pi\iota\sum_{k=1}^{n} RES[f, z_k]\,. \tag{18}$$

The illustration of such a situation is shown in Fig. 3, and the general form of the residue theorem can be expressed in Eq. (19).

$$RES f(x) = \frac{1}{2\pi\iota}\int_{-\infty}^{+\infty} f(x)\,dx. \tag{19}$$

The forward Euler method which is represented by Eq. (20), is implemented to ensure the convergence of the point to the reference point, so that the stability of the system is maintained [18, 19].

$$\dot{y} \approx \frac{y(t+h) - y(t)}{h}. \tag{20}$$

4.2 Using residual for speed controller

In this controller (Residual for speed controller), a speed control loop has been designed using the residue theorem where the dq-axis current controllers are controlled using PI controllers. The speed boundary area is selected to be between a reference point plus the absolute value of the error and the reference point minus the absolute value of the error. The speed error (e) is the difference between the reference point and the actual measured point of speed. The implementation of Eq. (19) to the speed controller is done by assuming that at each point of time the speed lies in the boundary between the reference speed (ω_{rref}) plus error and the reference speed minus error. The rotor speed can be expressed as follows:

$$RES(\omega_r) = \frac{1}{2\pi\iota}\int_{\omega_{rref-e}}^{\omega_{rref+e}} \omega_r\,d\omega. \tag{21}$$

By solving the above integration, the definition of the controlled speed can be described as:

$$RES(\omega_r) = \mid \frac{\omega_{rref}e}{\pi} \mid . \tag{22}$$

The speed error is defined according to the forward Euler method to ensure the convergence of the speed to the reference speed which is shown in Eq. (20).

$$\left.\begin{aligned} \dot{e} &= e + c \\ e &= \omega_{rref} - \omega_r \end{aligned}\right\} \tag{23}$$

By solving (23),

$$\dot{\omega}_{rref} - \dot{\omega}_r = \omega_{rref} - \omega_r + c \tag{24}$$

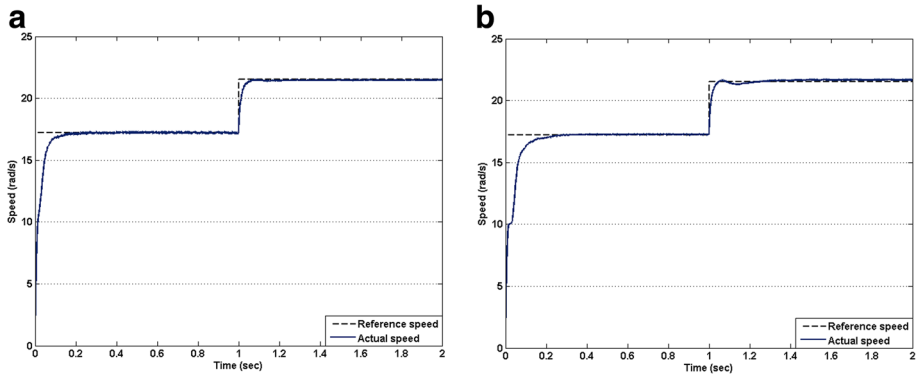

Fig. 5 Simulation results of the proposed controllers **a** Actual speed tracking the reference speed of Residual for speed controller. **b** Actual speed tracking the optimum speed of Residual for speed and currents controller

Solving (24) with respect to the mechanical speed Eq. (5) to get the final design equation, which is used to generate the q-axis reference current. Then the design equation is presented in (25).

$$i_q = \frac{3}{2p\psi_{PM}}\left[T_m - B\omega_r - \frac{J}{\pi}\omega_{rref} - JK\right]. \qquad (25)$$

4.2.1 Controller stability analysis

The stability of a controller is determined by implementing the forward Euler which ensures the convergence of the operating point to the boundary. The forward Euler converges strongly when the function is Lipschitz [19, 20]. Assume that wind speeds change from 8 m/s to 10 m/s then the reference speed, which is generated from an MPPT controller, changes from ω_{rref1} to ω_{rref2}. Hence the rate of change of the actual speed is as the following:

$$\dot{\omega}_r = \dot{\omega}_{rref} - \omega_{rref2} + \omega_{r1} - c. \qquad (26)$$

It should be noted that the term $\dot{\omega}_{rref}$ has the highest influence in the controller decision. Furthermore, the change in the actual speed has the same sign of the change

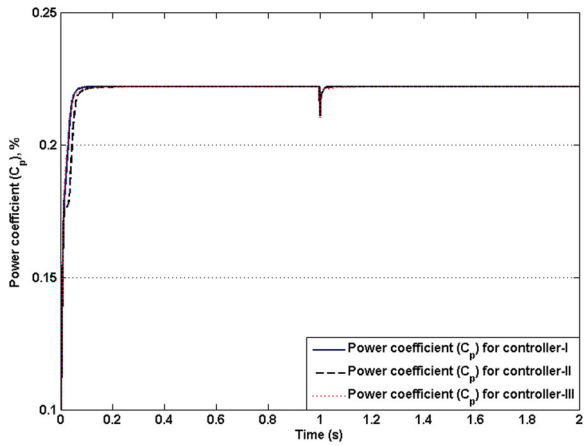

Fig. 6 Power coefficient C_p of WPGS with the proposed controllers

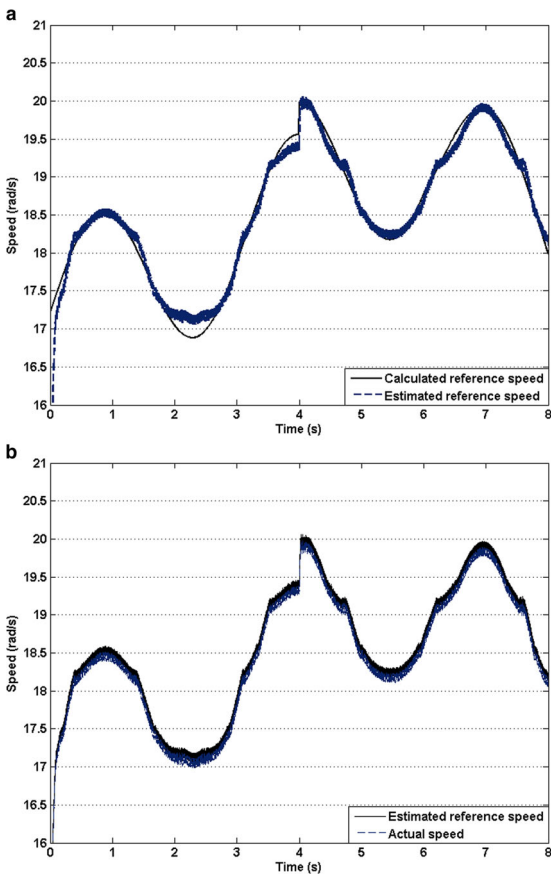

Fig. 7 Simulation result of the speed estimation **a** Calculated reference speed versus the Estimated reference speed. **b** Actual speed tracking the estimated reference speed of Residual for speed and currents controller

Table 1 Comparision between PI, SMC and Residual control

	PI	SMC	Residual control
Rise Time (ms)	29	53.7	52.5
Settling Time (ms)	250	230	210
Maximum Steady-States error (rad\s)	0.035	0.13	0.055
Low Speed Chattering (rad\s)	0.1	0.117	0.13
High Speed Chattering (rad\s)	0.088	0.098	0.093
Power coefficient (C_p)	0.2166	0.2167	0.2221

of the reference speed. The value of the constant c should ensure the convergence of the system and the stability and it must meet the following Lipschitz condition [21]:

$$c \leq \frac{|\dot{\omega}_r - \dot{\omega}_{rref}|}{|\omega_r - \omega_{rref}|}. \tag{27}$$

4.3 Using residual for speed and currents controller

In this controller (Residual for speed and currents controller), the speed and dq-axis current controller are designed using the residue theorem. The boundaries are selected to be the reference value plus the error and the reference value minus the error. The linearized dq-axis equations and the final design equations are shown in (28) [22].

$$\left.\begin{aligned} V_d &= R_s I_d + L\frac{di_d}{dt}, \\ V_q &= R_s I_q + L\frac{di_q}{dt}, \\ V_d &= R_s I_d + LK, \\ V_q &= R_s I_q + \frac{L\, e\, i_{qref}}{\pi} + LK. \end{aligned}\right\} \tag{28}$$

The exact value of a rotor position angle is required in order to implement a dq-axis model. Many techniques for estimating the rotor position have been reported [23, 24]. In this controller, a back-EMF observer has been used to estimate the rotor position, since the back-EMF is a function of the rotating speed. The sinusoidal back-EMF equation in the $\alpha - \beta$ coordinate can be denoted as follows [22]:

$$\left.\begin{aligned} e_\alpha &= L\frac{d}{dt} i_\alpha + R_s i_\alpha + V_\alpha, \\ e_\beta &= L\frac{d}{dt} i_\beta + R_s i_\beta + V_\beta, \end{aligned}\right\} \tag{29}$$

where $e_{\alpha\beta}$, $V_{\alpha\beta}$ and $i_{\alpha\beta}$ are the back emf, voltage and current of a PMSG in the $\alpha - \beta$ co-ordinate and L is the PMSG inductance. The rotor position θ can be estimated from Eq. (29) as follows [25]:

$$\hat{\theta} = \tan^{-1}\left(\frac{e_\alpha}{e_\beta}\right). \tag{30}$$

The values of the dq-axis voltages are used to generate a control signal of a pulse width modulation (PWM). The dq-axis voltages are normalized and compared with a triangular signal with an amplitude of 1 and a frequency of 20 kHz.

4.4 Using proposed residual controller with estimated reference speed

One of the most important issues in WPGS control is the measurement of the wind speed. The accuracy of the wind speeds measurement can not be ensured using a single anemometer. Also, the data recorded using SCADA system contain noticeable deviations which influence in the power conversion efficiency [26]. In this controller, the wind speed is estimated using MPPT algorithm, and the reference speed is generated using the estimated data. The wind power model which is expressed in Eqs. 2 and 3 can be solved for the wind speed and the P_m is assumed to be the output DC power. The estimated wind speed can be shown as the following:

$$V_w = \frac{-D_{21}\omega_r^2 \pm \sqrt{D_{21}^2\omega_r^4 - 4D11\omega_r\left(D_{31}\omega_r^3 - VI\right)}}{2D_{11}\omega_r}. \tag{31}$$

where $D_{11} = 0.0960$, $D_{21} = -0.0098$ and $D_{31} = -0.0040$. The MPPT controller is implemented in the proposed controller-II which is presented in Section 4.3.

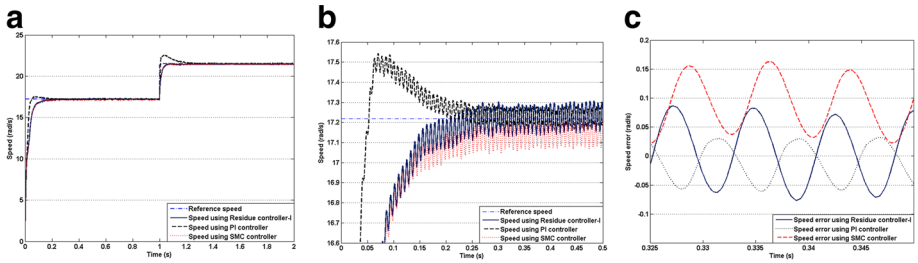

Fig. 8 Comparison between PI, SM and Residual controllers. **a** Speed response of PI, SM and Residual controllers. **b** Zoom in the speed response of PI, SM and Residual controllers. **c** Speed error of PI, SM and Residual controllers

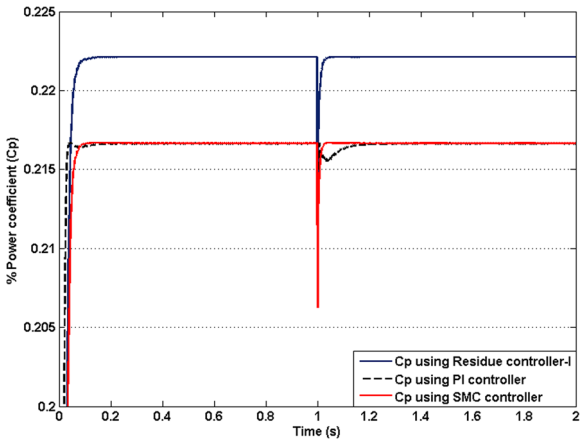

Fig. 9 Achieved C_p of PI, SM and Residual controllers

5 Simulation results and analysis

The control diagrams of the two developed MPPT controllers, i.e. Residual for speed controller and Residual for speed and currents controller are shown in Fig. 1a and b respectively. For both the controllers, the dq-model is obtained, and the measurement of wind speed is required. The PMSG voltage and current are measured, and the rotor position is required.

In this paper, the modelled wind turbine is a vertical axial wind turbine(VAWT), and the generator is a PMSG. The WPGS model has been simulated under variable wind speeds. The wind speed starts at 8 m/s then it goes to 10 m/s at t = 1 s. For each wind speed the controllers generate reference speed for optimal operation. The parameters of the PMSG and the VAWT employed in this simulation are illustrated in the Appendix, where the power rating is 500 W.

The two controllers have been simulated using MATLAB/SIMULINK. Figure 4 shows the speed dynamic boundary of the system. It is clear that the speed boundary is decreasing when the PMSG is accelerating. In addition, the integration effect makes the boundary limits changing soft. It can be noted that during transients, the dynamic boundary converges smoothly and fast enough to ensure the system robustness. Figures 5a shows the actual speed tracking the reference speed for the first proposed controller (Residual for speed controller). It is noticeable that the actual speed is accurately tracking the reference speed without any overshoots or steady-state errors. Also, the response speed is very fast and the settling time is at a satisfactory level.

Figure 5b shows the actual speed tracking the reference speed for the second proposed controller (Residual for speed and currents controller). It is noticeable that the actual speed is perfectly tracking the reference speed. There is a small overshoot appears in the speed response, which can be acceptable. The response speed is very fast and the settling time is at a satisfactory level.

The maximum conversion of power is ensured and clearly shown in Fig. 6. The C_p is at its maximum value of 0.22.

Figure 7 shows the actual rotor speed tracking the estimated reference speed generated from the MPPT algorithm. Also, the actual reference speed which is obtained from real wind measurement is shown in the figure. It is clear that the estimated reference speed is almost equal to the actual reference speed.

5.1 Comparison with PI and SMC

The proposed Residual for speed controller has been compared to a classical PI controller and a sliding mode controller. The comparison results are presented in Table 1 and Fig. 8. The residual controller is better than the PI and SMC in terms of achieving MPP. Figures 8a and 8b show the speed errors for the both controllers and a zoom in the speed error respectively. It can be seen that the speed error of the residual controller changing around zero, which means the rotor speed reaches the reference speed and varies around the designed speed boundary. Although, the speed response when using sliding mode controller reaches the reference speed perfectly. The speed error slide above zero. Moreover, the dynamic boundary of the residual controller is clearly at high speed as shown in Fig. 8a.

Figure 8c shows the speed response of the three controllers for time analysis. It can be seen that the controllers' actions are fast. The residual controller

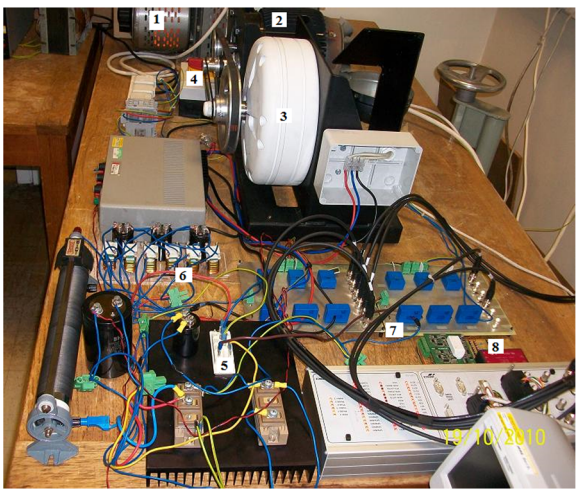

Fig. 10 Experimental set up for WPGS

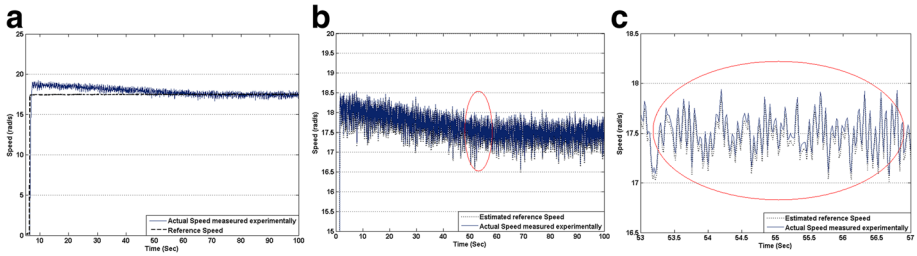

Fig. 11 Experimental test results at 8 m/s wind speed. **a** Actual speed tracking reference speed using wind speed measurements. **b** Actual speed tracking reference speed using wind speed estimator. **c** Zoom in the actual speed tracking reference speed using wind speed estimator

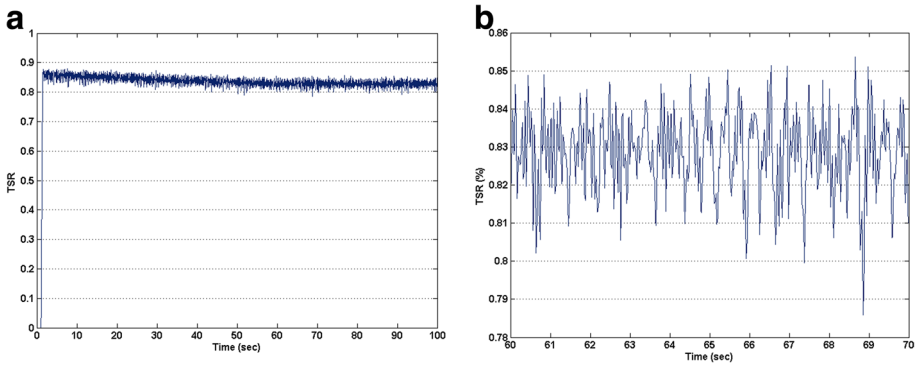

Fig. 12 Experimental test results. **a** Tip speed ratio λ at estimated (8 m/s) wind speed. **b** Zoom in the tip speed ratio λ at estimated (8 m/s) wind speed

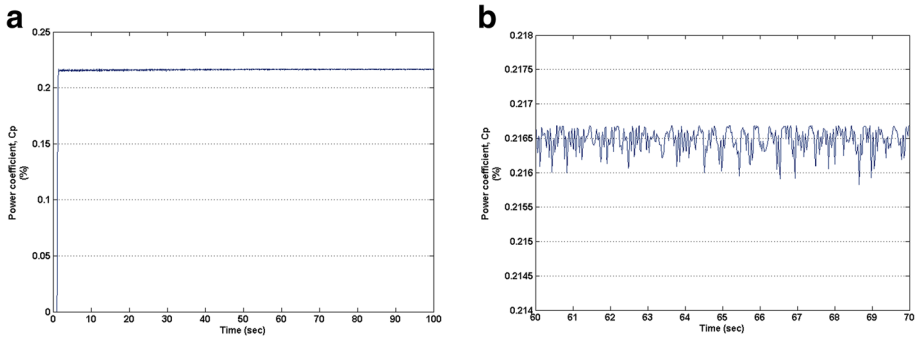

Fig. 13 Experimental test results. **a** Power coefficient C_p at estimated (8 m/s) wind speed. **b** Power coefficient C_p at estimated (8 m/s) wind speed

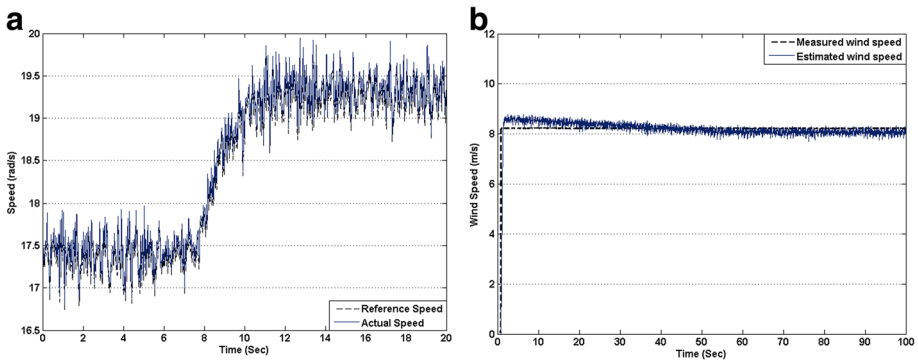

Fig. 14 Experimental test results at 8 m/s wind speed. **a** Actual speed tracking reference speed during a step change in wind speed from 8 to 10 m/s. **b** Actual wind speed versus estimated wind speed

rises faster than the SMC but slower than PI. The settling time for the residual controller is less than PI and SMC. It is worth to note that the residual controller has the highest power coefficient over other controllers as illustrated in Fig. 9. The power extracted when using the residual controller is 2.5% than when using SMC. The reason is that the rotor speed under residual controller slightly varies around the zero, which can be an advantage of introducing the dynamic boundary.

According to Table 1, the chattering effect of SMC at low speed is less than the residual controller. However, at high speed, the chattering effect reduces in the residual controller and increases in the SMC. It can be concluded that the residual controller has advantages over both PI and SMC, i.e. more power efficient, better dynamic performance, simple structure and implementation. Although, the SMC is simple structure control. It can be more complicated to overcome the chattering effect.

6 Experimental verifications

The experimental tests have been conducted using a WPGS test bench shown in Fig. 10. The WPGS test bench consists of PMSG coupled with a 3-phase induction motor, which approximates the wind speeds in terms of mechanical torque. The 3-phase outputs of the PMSG are connected to a DC-DC boost converter to supply a resistive load. The measurements and control system are sampled and implemented by dSPACE DS1104 controller. Voltage and current transducers are used for measurement where an encoder is used for speed measurements. The experimental tests have been performed under two level of wind speeds 8 m/s and 10 m/s focusing in the transients response. The wind speed estimator was tested and implemented in the controller.

6.1 Experimental results and analysis

The actual speed tracking the reference speed at a wind speed of 8 m/s is shown in Fig. 11a. It can be seen that the proposed controller tracks the reference value. It is important to note that the soft changing dynamics caused by the controller allows a time to settle the generator which can prevent a mechanical stress on the drive train. The discussed wind speed estimator has been implemented in the control system. The results are presented in Figs. 11b and 11c. The optimal TSR has been achieved as shown in Figs. 12a and 12b. The power coefficient, which is illustrated in Fig. 13a indicates a maximum power conversion ability of 0.216, where the theoretical maximum value of C_p is 0.22. Figure 13b gives a clear picture of the achieved power coefficient. It is shown that the performance of the WPGS was enhanced when using wind speed estimator in terms of settling time and overshoots. The transients response is shown in Fig. 14a. It shows actual speed tracking the reference speed during a step change in wind speed from 8 to 10 m/s. It was clear that the controller perfectly reacts with a varying reference signal and maintains the desired action in fast and smooth manner. Finally, the performance of the wind speed estimator during the experimental verification is shown in Fig. 14b, in which the actual wind speed perfectly match the estimated one.

7 Conclusion

In this paper, a control method based on the residue theorem has been developed for WPGS. By creating a soft boundary around a reference point, the control variables are controlled to lie inside the boundary instead of a particular value. two types of controllers have been designed. For both controllers, the convergence of the manipulating variable to the set point is calculated by the forward Euler method, where the exponential function ensures the convergence for the third controller. The two proposed controllers have been simulated and tested experimentally to validate the control scheme. The soft control strategy developed provides a stable operation which can be partially lost when changing the discontinuity behavior of SMC. The overshoot is completely absent, and the response speed is fast and soft enough. It can be concluded that using the residue control method with the combination of PI controller improves the dynamics performance for the PMSG based WPGS.

The experimental results as well as the simulation results, which is shown in Table 1, show that the proposed controller overcome the limitations of PI and SMC control in terms of overshoots and energy conversion efficiency. Also, a wind speed estimation algorithm has been introduced in this study. It can be concluded that the dynamic performance of the system and the energy conversion ratio have been improved when using the estimated value of the wind speed. Besides, a comparative study between PI, SMC and residual controllers has been presented. Based on the comparison, the residual controller shows improved dynamic performance and higher energy conversion ratio than both PI and SMC.

It can be concluded that this method has been proposed and implemented in VAWT and it can be also implemented in other system as there is no specific design limitations shown. That is because the method is proposed based on mathematical theory and is not a system based. Although, the investigated system is of small-scale, the implementation of the proposed control technique to a medium and large scale system is considered in future.

Appendix

Table 2 Nomenclature

P_w:	Wind turbine power	P_m:	Extracted mechanical power
ψ_{PM}:	Permanent magnet flux	S:	Sliding surface
i_{dq}:	Direct and quadrature currents	C_p:	Power coefficient
$\omega_{r,e}$:	Mechanical and electrical speeds	λ:	Tip speed ratio
R:	Radius of the wind turbine rotor	ρ:	Air density
V_{dq}:	Direct and quadrature voltages	V_w:	Wind speed
L_{dq}:	Direct and quadrature inductance	R_s:	Stator resistance
$T_{m,e}$:	Mechanical and electrical torques	e:	Error
B:	Viscus friction coefficient	J:	PMSG inertia
A:	Swept area of the wind turbine	γ:	Positive constant matrix
$V_{\alpha\beta}$:	PMSG voltage in $\alpha - \beta$ coordinate	x_{ref}:	Reference Value
$e_{\alpha\beta}$:	PMSG back-EMF in $\alpha - \beta$ coordinate	x:	Controlled variable
$i_{\alpha\beta}$:	PMSG current in $\alpha - \beta$ coordinate	L:	PMSG inductance
y:	Controlled variable	h:	Step size
$K_{,\omega,d,q}$, Y, Z, k and c: Constants			

Table 3 Parameters of the WPGS

Parameters	Value
VAWT	
Type	Savonius VAWT
Maximum Power Coefficient	0.22
Optimal TSR	0.82
PMSG	
Type	GL-PMG500A
Rated Power	500 W
Stator Winding Resistance	0.35 Ω
Moment of Inertia	0.066 $Kg.m^2$

Acknowledgments
The author would like to thank the Royal commission for Jubail and Yanbu and the University of Liverpool for providing the financial support for this study.

Funding
This study has been funded by the Royal Commission for Jubail and Yanbu, Saudi Arabia and the University of Liverpool, UK.

Availability of data and materials
The datasets used and/or analysed during the current study are available from the corresponding author on reasonable request.

Authors' contributions
MA, the main author of this study his contributions toward the idea, mathematical and practical design, analysis, and proof of the idea, test and writing the paper.
LL, the corresponding author her contribution toward the practical test setup and measurements, revising and improving the text.
LJ and WT, the supervisors of the study their contributions toward supervising and guiding the study at all stages, reviewing and improving the text. All authors read and approved the final manuscript.

Competing interests
The authors declare that they have no competing interests.

Received: 20 October 2017 Accepted: 21 June 2018
Published online: 08 August 2018

References

1. Johnson, KE, Pao, LY, Balas, MJ, Fingersh, LJ (2006). Control of variable-speed wind turbines: standard and adaptive techniques for maximizing energy capture. *IEEE Control Syst*, *26*(3), 70–81.
2. Howlader, AM, Urasaki, N, Yona, A, Senjyu, T, Saber, AY (2013). Design and implement a digital h robust controller for a mw-class pmsg-based grid-interactive wind energy conversion system. *Energies*, *6*, 42084–2109.
3. Koutroulis, E, & Kalaitzakis, K (2006). Design of a maximum power tracking system for wind-energy-conversion applications. *IEEE Trans Ind Electron*, *53*(2), 486–494.
4. Hu, J, Nian, H, Hu, B, He, Y, Zhu, ZQ (2010). Direct active and reactive power regulation of dfig using sliding-mode control approach. *IEEE Trans Energy Convers*, *25*(4), 1028–1039.
5. Fridman, L, & Levant, A (2002). Higher order sliding modes. *Sliding Mode Control Eng*, *11*, 53–102.
6. Burton, T, Jenkins, N, Sharpe, D, Bossanyi, E (2011). *Wind Energy Handbook*. Hoboken: Wiley.
7. Morimoto, S, Nakamura, T, Takeda, Y (2003). Power maximization control of variable speed wind generation system using permanent magnet synchronous generator. *IEEJ Trans Power Energy*, *123*, 1573–1579.
8. Jiang, S, Liang, J, Y-d Liu, Yamazaki, K, Fujishima, M (2005). Modeling and cosimulation of fpga-based svpwm control for pmsm, In *Industrial Electronics Society, 2005. IECON 2005. 31st Annual Conference of IEEE*. https://doi.org/10.1109/IECON.2005.1569133 (pp. 6–pp): IEEE.
9. Zentai, A, & Dabóczi, T (2005). Improving motor current control using decoupling technique, In *Computer as a Tool, 2005. EUROCON 2005. The International Conference on, vol. 1*. https://doi.org/10.1109/EURCON.2005.1629934 (pp. 354–357). Belgrade: IEEE.
10. Åström, KJ, & Hägglund, T (2006). *Advanced PID control*. Research Triangle Park: ISA-The Instrumentation, Systems, and Automation Society.
11. Datta, R, & Ranganathan, V (2003). A method of tracking the peak power points for a variable speed wind energy conversion system. *IEEE Trans Energy Convers*, *18*(1), 163–168.
12. Vrdoljak, K, Perić, N, Petrović, I (2010). Sliding mode based load-frequency control in power systems. *Electr Power Syst Res*, *80*(5), 514–527.
13. Bandyopadhyay, B, Deepak, F, Kim, K-S (2009). Sliding mode control using novel sliding surfaces, vol. 392. https://doi.org/10.1007/978-3-642-03448-0.
14. Castaños, F, & Fridman, L (2006). Analysis and design of integral sliding manifolds for systems with unmatched perturbations. *IEEE Trans Autom Control*, *51*(5), 853–858.
15. Europe Texas Instruments (1998). Field orientated control of 3-phase ac-motors. *Literature Number: BPRA073*.

16. Bak, J, & Newman, DJ (2010). Complex analysis, In *Complex Analysis* (pp. 1–20). New York: Springer.
17. Cattani, E, & Dickenstein, A (2005). Introduction to residues and resultants, In *Solving polynomial equations*. ISBN:3540243267 (pp. 1–61). Heidelberg: Springer-Verlag Berlin.
18. Sandberg, M (2008). Convergence of the forward euler method for nonconvex differential inclusions. *SIAM J Numer Anal*, *47*(1), 308–320.
19. Higham, DJ, Mao, X, Stuart, AM (2002). Strong convergence of euler-type methods for nonlinear stochastic differential equations. *SIAM J Numer Anal*, *40*(3), 1041–1063.
20. Bjørhus, M (1995). A note on the convergence of discretized dynamic iteration. *BIT Numer Math*, *35*(2), 291–296.
21. Eriksson, K, Estep, D, Johnson, C (2004). Applied Mathematics: Body and Soul, 517–519. https://doi.org/10.1007/978-3-662-05798-8_7.
22. Mahdi, AJ (2011). *Development of novel sensorless maximum power point tracking controllers for wind turbine generator systems, Ph.D. dissertation*. Liverpool: University of Liverpool.
23. Senjyu, T, Tamaki, S, Urasaki, N, Uezato, K, Funabashi, T, Fujita, H (2003). Wind velocity and position sensorless operation for pmsg wind generator, In *Power Electronics and Drive Systems, 2003. PEDS 2003. The Fifth International Conference on Power Electronics and Drive Systems, 2003. PEDS 2003, vol. 1*. https://doi.org/10.1109/PEDS.2003.1283005 (pp. 787–792): IEEE.
24. Harnefors, L, & Nee, H-P (2000). A general algorithm for speed and position estimation of ac motors. *IEEE Trans Ind Electron*, *47*(1), 77–83.
25. Zhao, Y, Qiao, W, Wu, L (2012). Position extraction from a discrete sliding-mode observer for sensorless control of ipmsms, In *Industrial Electronics (ISIE), 2012 IEEE International Symposium on Industrial Electronics* (pp. 725–730). Hangzhou: IEEE.
26. Wang, Y, Infield, DG, Stephen, B, Galloway, SJ (2013). *Copula-based model for wind turbine power curve outlier rejection, Wind Energy*. Wiley. https://doi.org/10.1002/we.1661.